Inorg. Chem. **2008**, *47*, 10587−10599

Mechanism of Pyridine−Ligand Exchanges at the Different Labile Sites of 3d Heterometallic and Mixed Valence μ_3-oxo Trinuclear Clusters

Ghenadie Novitchi,*,‡,§ Fabrice Riblet,§ Rosario Scopelliti,§ Lothar Helm,*,§ Aurelian Gulea,# and André E. Merbach*,§

Institute of Chemistry, Academy of Sciences of Moldova, Academiei str. 3. MD-2028 Chisinau, Moldova, Laboratoire de Chimie Inorganique et Bioinorganique, Ecole Polytechnique Fédérale de Lausanne, CH-1015 Lausanne, Switzerland, and Department of Chemistry Moldova State University, A. Mateevici str. 60, MD-2009 Chisinau, Moldova

Received July 1, 2008

The syntheses and single crystal X-ray structural analysis of five novel hetero- and homometallic μ_3-oxo trinuclear cluster with the formula $[Fe^{III}_2M^{II}(\mu_3\text{-}O)(\mu\text{-}O_2CCH_3)_6(4\text{-Rpy})_3]\cdot x(4\text{-Rpy})\cdot y(CH_3CN)$ where R = Ph for **1**(Fe_2Mn), **2**(Fe_2Fe), **3**(Fe_2Co), **4**(Fe_2Ni) and R = CF_3 for **5**(Fe_2Co), are reported. The persistence of the structure for compounds **2**−**5** in dichloromethane solution in the temperature range 190−320 K is demonstrated by ^1H and ^{19}F NMR spectroscopy. Even at the lowest temperature, the electron exchange in the homometallic mixed-valence compound **2**(Fe_2Fe) is in the fast regime at the NMR time scale. Variable temperature and pressure NMR line broadening allowed quantifying the fast coordinated/free 4-Rpy exchanges at the two labile metal centers in these clusters: **2**: Fe^{III}($k^{298}/10^3$ s^{-1} = 16.6; $\Delta H^{\ddagger}$ = 60.32 kJ mol^{-1}; $\Delta S^{\ddagger}$ = + 34.8 J K^{-1} mol^{-1}; $\Delta V^{\ddagger}$ = + 12.5 cm^3 mol^{-1}); **3**: Fe (11.9; 58.92; +30.7; +10.6) and Co (2.8; 68.24; +49.8; +13.9); **4**: Fe(12.2; 67.91; +61.0; −) and Ni (0.37; 78.62; +67.8; +12.3); **5**: Fe (46; 58.21; +39.3; +14.2) and Co (4.7; 55.37; +11.2; +10.9). A limiting D mechanism is assigned to these exchange reactions. This assignment is based on a first-order rate law, the detection of intermediates, the positive and large entropies and volumes of activation. The order of reactivity $k^{Co} > k^{Ni}$ is expected for a D mechanism at these metal centers: their low exchange rates are due to their strong binding with the 4-Rpy donor. Surrounded by oxygen donors the d^5 iron(III) usually reacts associatively; however, here due to low affinity of this ion for nitrogen the mechanism is D and the rate of exchange is very fast, even faster than on the divalent ions. There is no significant effect of the divalent ion in cluster **2**, **3**, and **5** on the exchange rates of 4-Phpy at the iron center, which seems to indicate that the specific electronic interactions between the three ions making the clusters do not influence the Fe^{III}−N bond strength.

1. Introduction

Solvent exchange reactions on metal cations are among the simplest chemical reactions. They are considered as fundamental reactions for metal ions in solution, in particular for the understanding of complex-formation reactions and of redox processes.[1−6] Only a few experimental techniques are available to determine solvent exchange rate constants directly. Nuclear magnetic resonance (NMR) spectroscopy has shown the widest range of application. For example, variable pressure oxygen-17 NMR revealed the progressive changeover in the water exchange mechanism for high-spin divalent and trivalent 3d octahedral aqua ions.[7,8] As the

* To whom correspondence should be addressed. Phone: 0041 21 693 9875. Fax: 0041 21 693 9871. E-mail: lothar.helm@epfl.ch.
‡ Academy of Sciences of Moldova.
§ Ecole Polytechnique Fédérale de Lausanne.
# Moldova State University.

(1) Lincoln, S. F.; Richens, D. T.; Sykes, A. G. In *Comprehensive Coordination Chemistry II*; McCleverty, J. A.; Meyer, T. J., Eds.; Elsevier: Oxford, 2004; Vol. 1, pp 515−555.
(2) Tobe, M. L.; Burgess, J. *Inorganic Reaction Mechanisms*; Longman: New York, 1999.
(3) Richens, D. T. *Chem. Rev.* **2005**, *105*, 1961–2002.
(4) Dunand, F. A.; Helm, L.; Merbach, A. E. *Adv. Inorg. Chem.* **2003**, *54*, 1–69.
(5) Helm, L.; Merbach, A. E. *Chem. Rev.* **2005**, *105*, 1923–1960.
(6) Funahashi, S.; Inada, Y. *Bull. Chem. Soc. Jpn.* **2002**, *75*, 1901–1925.
(7) Helm, L.; Merbach, A. E. In *High Pressure Chemistry*; van Eldik, R.; Klärner, F.-G., Eds.; Wiley-VCH: Weinheim, 2002; pp 131−160.
(8) Helm, L.; Merbach, A. E. *J. Chem. Soc., Dalton Trans.* **2002**, 633–641.

10.1021/ic801206m CCC: $40.75 © 2008 American Chemical Society
Published on Web 10/21/2008

number of d electrons increases and the ionic radii decrease along the 3d series the mechanism changes from an associative interchange I_a to a dissociative I_d mechanism after the d^5 configuration.[5,9] This was inferred from the values and the change in sign of the activation volumes. The rates of water exchange on metal ions covers almost 20 orders of magnitude.[5] The difference of reactivity between labile and inert complexes was largely used to assign inorganic reaction mechanisms. For example, the water exchange rate of Cr^{III} is one of the lowest, but Cr^{II} is extremely labile. This significant difference in reactivity of chromium complexes was used to demonstrated the mechanism of electron transfer.[10−12] Another example concerns Co^{III} and Co^{II}, which shows also a large increase in reactivity from their inert low spin trivalent to their labile high spin bivalent complexes.[13]

This situation can be changed in hetero- and homometallic cluster compounds and also in nanoparticles where metal−metal magnetic interactions modify the electronic structure and the metal−ligand chemical bonding.[14] These type of species are interesting models for surface structures and kinetics in heterogeneous catalysis, for molecular geochemistry, bioinorganic chemistry, etc.[15−18] Among the clusters, the family of hetero- and homometallic μ_3-oxo trinuclear compounds $[M^{III}_2M^{II}(\mu_3\text{-}O)(\mu\text{-}O_2CR)_6L_3]$ (where ^-O_2CR is a bridging ligand and L is a monodentate ligand coordinated to a metal center) is fascinating. An immense variety of compounds of this family with different combinations of metals and ligands L (H_2O, pyridines, etc.) have been studied in the solid state from a structural point of view and also for their magnetic properties.[19−45] However, solution kinetic studies have been performed only on a few of them, mostly chosen for their inertness, as for example: $[M_3(\mu_3\text{-}O)(\mu\text{-}O_2CR)_6L_3]^+$ for M = Cr^{III}, Ru^{III}, Rh^{III} and L = H_2O, Py.[46−53] In these trinuclear monocataionic species the kinetic behavior dramatically differs from that observed in the corresponding trivalent hexaaqua ions: faster water exchange rates, and D exchange mechanisms instead of I_a were observed. This was assigned to a *trans* effect of the central oxide ion and to additional *cis* effects of the bridging carboxylates.[46]

The goal of our study is to analyze the kinetic behavior of labile 3d heterometallic and mixed valence clusters. We report the syntheses and X-ray structural analysis of five novel hetero- and homometallic μ_3-oxo trinuclear clusters of general formula $[Fe^{III}_2M^{II}(\mu\text{-}O_2CCH_3)_6(4\text{-}Rpy)_3]$, where R = Ph for **1** (Fe_2Mn), **2**(Fe_2Fe), **3**(Fe_2Co), **4**(Fe_2Ni) and R = CF_3 for **5**(Fe_2Co). The absence of charge and the choice 4-Rpy lead to a good solubility in dichloromethane, a suitable solvent to easily follow the fast coordinated/free ligand exchange by ^1H and ^{19}F NMR line broadening at variable temperature and pressure. The paramagnetic ions making up

(9) van Eldik, R.; Merbach, A. E. *Comments Inorg. Chem.* **1992**, *12*, 341–378.
(10) Craft, R. W.; Gaunder, R. G. *Inorg. Chem.* **1975**, *14*, 1283–1289.
(11) Craft, R. W.; Gaunder, R. G. *Inorg. Chem.* **1974**, *13*, 1005–1008.
(12) Taube, H.; Gaunder, R. G. *Inorg. Chem.* **1970**, *9*, 2627–2639.
(13) Haim, A. *Prog. Inorg. Chem.* **1983**, *30*, 273–357.
(14) Balogh, E.; Casey, W. H. *Prog. NMR Spectrosc.* **2008**, *53* (4), 193–207.
(15) Casey, W. H. *Chem. Rev.* **2006**, *106*, 1–16.
(16) Casey, W. H.; Rustad, J. R. *Annu. Rev. Earth Planet. Sci.* **2007**, *35*, 21–46.
(17) Wang, J.; Rustad, J. R.; Casey, W. H. *Inorg. Chem.* **2007**, *46*, 2962–2964.
(18) Casey, W. H.; Olmstead, M. M.; Phillips, B. L. *Inorg. Chem.* **2005**, *44*, 4888–4890.
(19) Nakata, K.; Nagasawa, A.; Soyoma, N.; Sasaki, Y.; Ito, T. *Inorg. Chem.* **1991**, *30*, 1575–1579.
(20) Sasaki, Y.; Tokiwa, A.; Ito, T. *J. Am. Chem. Soc.* **1987**, *109*, 6341–6347.
(21) Nakamoto, T.; Hanaya, M.; Katada, M.; Endo, K.; Kitagawa, S.; Sano, H. *Inorg. Chem.* **1997**, *36*, 4347–4359.
(22) Sato, T.; Ambe, F.; Endo, K.; Katada, M.; Maeda, H.; Nakamoto, M.; Sano, H. *J. Am. Chem. Soc.* **1996**, *118*, 3450–3458.
(23) Sorai, M.; Kaji, K.; Hendrickson, D. N.; Oh, S. M. *J. Am. Chem. Soc.* **1986**, *108*, 702–708.
(24) Andras, M. T.; Duraj, S.; Hepp, A. F.; Fanwick, P. E.; Bodnar, M. M. *J. Am. Chem. Soc.* **1992**, *114*, 786–787.
(25) Oh, S. M.; Hendrickson, D. N.; Hassett, K. L.; Davis, R. E. *J. Am. Chem. Soc.* **1984**, *106*, 7984–7985.
(26) Sorai, M.; Shiomi, Y.; Hendrickson, D. N.; Oh, S. M.; Kambara, T. *Inorg. Chem.* **1987**, *26*, 223–230.
(27) Dziobkowski, C. T.; Wrobleski, J. T.; Brown, D. B. *Inorg. Chem.* **1981**, *20*, 679–684.
(28) Meesuk, L.; Jayasooriya, U. A.; Cannon, R. D. *J. Am. Chem. Soc.* **1987**, *109*, 2009–2016.
(29) Oh, S. M.; Wilson, S. R.; Hendrickson, D. N.; Woehler, S. E.; Wittebort, R. J.; Inniss, D.; Strouse, C. E. *J. Am. Chem. Soc.* **1987**, *109*, 1073–1090.
(30) Oh, S. M.; Hendrickson, D. N.; Hassett, K. L.; Davis, R. E. *J. Am. Chem. Soc.* **1985**, *107*, 8009–8018.
(31) Wu, C.-C.; Hunt, S. A.; Gantzel, P. K.; Gutlich, P.; Hendrickson, D. N. *Inorg. Chem.* **1997**, *36*, 4717–4733.
(32) Wu, C.-C.; Jang, H. G.; Rheingold, A. L.; Gutlich, P.; Hendrickson, D. N. *Inorg. Chem.* **1996**, *35*, 4137–4147.
(33) Wilson, C.; Iversen, B. B.; Overgaard, J.; Larsen, F. K.; Wu, G.; Palii, S.; Timco, G. A.; Gerbeleu, N. V. *J. Am. Chem. Soc.* **2000**, *122*, 11370–11379.
(34) Cannon, R. D.; Jayasooriya, U. A.; Montri, L.; Saad, A. K.; Karu, E.; Bollen, S. K.; Sanderson, W. R.; Powell, A. K.; Blake, B. B. *J. Chem. Soc., Dalton Trans.* **1993**, 2005–2010.
(35) Edwards, A. B.; Charnock, J. M.; Garner, C. D.; Blake, B. B. *J. Chem. Soc., Dalton Trans.* **1995**, 2515–2518.
(36) Vincent, J. B. *Inorg. Chem.* **1994**, *33*, 5604–5606.
(37) Bino, A.; Cotton, A.; Dori, Z.; Koch, S.; Kuppers, H.; Millar, M.; Sekutowski, J. C. *Inorg. Chem.* **1978**, *17*, 3245–3253.
(38) Schake, A. R.; Vincent, J. B.; Li, Q.; Boyd, P. D. W.; Folting, K.; Huffman, J. C.; Hendrickson, D. N.; Christou, G. *Inorg. Chem.* **1989**, *28*, 1915–1923.
(39) White, R. P.; Stride, J. A.; Bollen, S. K.; Sa-Ard, C. N.; Kearley, G. J.; Jayasooriya, U. A.; Cannon, R. D. *J. Am. Chem. Soc.* **1993**, *115*, 7778–7782.
(40) Vincent, J. B.; Chang, H. R.; Folting, K.; Huffman, J. C.; Christou, G.; Hendrickson, D. N. *J. Am. Chem. Soc.* **1987**, *109*, 5703–5711.
(41) Ardon, M.; Bino, A.; Cotton, A.; Dori, Z.; Kaftory, M.; Reisner, G. *Inorg. Chem.* **1982**, 21.
(42) Cotton, A.; Dori, Z.; Marler, D. O.; Schowotzer, W. *Inorg. Chem.* **1983**, *22*, 3104–3106.
(43) Bino, A.; Cotton, A.; Dori, Z.; Shaia-Gottlieb, M.; Kapon, M. *Inorg. Chem.* **1988**, 3592–3596.
(44) Blake, A. B.; Yavari, A. *J. Chem. Soc., Chem. Commun.* **1982**, 1247–1249.
(45) McCusker, J. K.; Jang, H. G.; Wang, S.; Christou, G.; Hendrickson, D. N. *Inorg. Chem.* **1992**, *31*, 1874–1880.
(46) Fujihara, T.; Aonahata, J.; Kumakura, S.; Nagasawa, A.; Murakami, K.; Ito, T. *Inorg. Chem.* **1998**, *37*, 3779–3784.
(47) Fujihara, T.; Yasui, M.; Ochikoshi, J.; Terasaki, Y.; Nagasawa, A. *Inorg. React. Mech.* **2000**, *2*, 119–128.
(48) Abe, Y.; Tanaka, M.; Umakoshi, K.; Sasaki, Y. *Inorg. Chem.* **1999**, *38*, 4146–4148.
(49) Sasaki, Y.; Nagasawa, A.; Tokiwa-Yamamoto, A.; Ito, T. *Inorg. Chim. Acta* **1993**, *212*, 175–182.
(50) Houston, H. R.; Casey, W. H. *Dalton. Trans.* **2005**, 3667–3671.
(51) Houston, H. R.; Yu, P.; Casey, W. H. *Inorg. Chem.* **2005**, *44*, 5176–5182.
(52) Houston, H. R.; Oimstead, M. M.; Casey, W. H. *Inorg. Chem.* **2006**, *45*, 7799–7805.
(53) Powell, G.; Richens, D. T.; Powell, A. K. *Inorg. Chim. Acta* **1993**, *213*, 147–155.

Table 1. Crystallographic Data for **1**−**5**

	1(Fe_2Mn)	**2**(Fe_2Fe)	**3**(Fe_2Co)	**4**(Fe_2Ni)	**5**(Fe_2Co)
chemical formula	$C_{45}H_{45}Fe_2MnN_3O_{13}\cdot 0.35C_{11}H_9N\cdot 3.3C_2H_3N$	$C_{45}H_{45}Fe_3N_3O_{13}\cdot 0.35C_{11}H_9N\cdot 3.3C_2H_3N$	$C_{45}H_{45}CoFe_2N_3O_{13}\cdot C_{11}H_9N\cdot 2C_2H_3N$	$C_{45}H_{45}Fe_2N_3NiO_{13}\cdot 5C_2H_3N$	$C_{30}H_{30}CoF_9Fe_2N_3O_{13}\cdot 4C_2H_3N$
formula weight	1192.28	1193.19	1243.77	1211.52	1146.42
crystal system	monoclinic	monoclinic	monoclinic	triclinic	monoclinic
space group	*C*2/*m*	*C*2/*m*	*C*2/*m*	$P\bar{1}$	*C*2/*c*
a (Å)	20.310(5)	20.3457(4)	20.318(4)	11.3576(15)	28.346(2)
b (Å)	26.330(5)	26.1592(6)	26.597(5)	16.5028(16)	16.3447(16)
c (Å)	11.114(3)	11.1804(3)	11.162(2)	16.6957(16)	22.435(3)
α (deg)	90	90	90	105.040(8)	90
β (deg)	98.85(3)	98.642(2)	97.12(3)	96.423(10)	110.109(9)
γ (deg)	90	90	90	92.983(9)	90
vol (Å^3)	5872(3)	5883.0(2)	5985(2)	2992.4(6)	9760.5(17)
Z	4	4	4	2	8
D_{calc} (g cm^{-3})	1.349	1.347	1.380	1.345	1.560
F(000)	2473	2477	2580	1260	4664
μ (mm^{-1})	0.765	0.795	0.819	0.855	1.023
temp (K)	140(2)	140(2)	100(2)	140(2)	140(2)
wavelength (Å)	0.71073	0.71073	0.71073	0.71073	0.71073
measured reflections	19147	23873	39281	17871	27456
unique reflections	5311	5323	5368	9253	8582
unique reflections [$I > 2\sigma(I)$]	2453	4188	4087	6350	4809
data/parameters	5311/441	5323/537	5368/415	9253/681	8582/652
R^a [$I > 2\sigma(I)$]	0.0839	0.0395	0.0776	0.0816	0.0738
$wR2^a$ (all data)	0.2452	0.1130	0.2299	0.2594	0.2157
GoF^b	0.928	1.111	1.126	1.062	0.969

^{a} $R = \Sigma||F_o| - |F_c||/\Sigma|F_o|$, wR2 = $\{\Sigma[w(F_o^2 - F_c^2)^2]/\Sigma[w(F_o^2)^2]\}^{1/2}$. ^{b} GoF = $\{\Sigma[w(F_o^2 - F_c^2)^2]/(n - p)\}^{1/2}$ where *n* is the number of data and *p* is the number of refined parameters.

these clusters show intramolecular interactions which modify their individual electronic structures and possibly the metal−ligand 4-Rpy bonding and ultimately the ligand exchange reactivity. Among these clusters, the mixed valence compound **2**(Fe_2Fe) is of particular interest due to the fast intramolecular electron exchange. This process has been shown to be slow in the solid state at the Mössbauer[21,22,27,54] and IR[55−58] time scales but has always been observed to be fast in solution at room temperature at the NMR time scale.[55,56]

2. Experimental Section

2.1. Synthesis. All chemicals and solvents were purchased from Aldrich and used without further purification. The heterometallic and mixed-valence trinuclear complexes $[Fe^{III}_2M^{II}(\mu_3\text{-}O)_6(4\text{-}Rpy)_3]\cdot x(4\text{-}Phpy)\cdot y(CH_3CN)$ (M = Mn, Fe, Co, Ni) where prepared in two steps: first the trinuclear aqua complexes $[Fe^{III}_2M^{II}(\mu_3\text{-}O)(\mu\text{-}O_2CCH_3)_6(H_2O)_3]$[28,32] and second the substitution of water by 4-phenylpyridine or by 4-trifluoromethylpyridine, in acetonitrile solution at 50−60 °C. The substitution procedure and all manipulations of the mixed valence compound **2**(Fe_2Fe) were made in a N_2 atmosphere glovebox. The deuterated compound $[Fe^{III}_2Fe^{II}(\mu_3\text{-}O)(\mu\text{-}O_2CCD_3)_6(4\text{-}Phpy)_3]$ (**2***) was obtained using deuterated derivates (CD_3CO_2D and CD_3COONa). The X-ray crystal structures (Table 1 and Figure 1) of the compounds were confirmed in solution by NMR integration of the acetate and pyridine ligand protons in the presence of added ligand. The Fe(III)/M(II) molar ratios were verified by ICP analysis for the heterometallic clusters used in the mechanistic study: 2.02 for **3**(Fe_2Co), 2.00 for **4**(Fe_2Ni), and 2.00 for **5**(Fe_2Co). IR spectra are given in the Supporting Information (Figure S1). The crystals used for the X-ray analysis were directly taken from acetonitrile solutions, to minimize degradation with loss of lattice acetonitrile.

2.2. X-ray Crystal Measurements. Data collections for all compounds have been obtained at low temperature using Mo Kα radiation. The equipment used was an Oxford Diffraction Sapphire/KM4 CCD (**1**, **2**, **4** and **5**) and a Bruker APEX II CCD (**3**) having both kappa geometry goniometers. Data were reduced by Crysalis PRO[59] (**1**, **2**, **4**, and **5**) and EvalCCD[60] (**3**). Semiempirical[61] absorption correction was applied to two data sets (**2** and **3**). Structure solutions and refinements have been carried out by SHELXTL.[62] Crystal structures were refined using full-matrix least-squares on F^2 with all non-H atoms anisotropically defined (except for disordered solvent molecules). The hydrogen atoms were placed in calculated positions by means of the "riding" model. Disorder problems concerning the phenyl ring of the pyridine ligands, some bridging acetates as well as the solvent molecules have been found in all structures. These disorders have been treated using the split model in the case of the phenyl rings or the acetates, whereas in the case of the solvent it has been treated by means of an isotropic and restrained (DFIX) treatment.

2.3. NMR Measurements. All samples were prepared under N_2 atmosphere by weighing the complexes directly in 5 mm NMR tubes and adding 0.50 mL of CD_2Cl_2. The ^{1}H chemical shifts were referred to TMS using the residual signals from the solvent $CHDCl_2$ (5.32 ppm). The concentrations of the complexes were about 10 mM and an excess of 4-Rpy was used in order to follow the ligand exchange process and to avoid a possible dissociation of the cluster

(54) Woehler, S. E.; Wittebort, R. J.; Oh, S. M.; Hendrickson, D. N.; Inniss, D.; Strouse, C. E. *J. Am. Chem. Soc.* **1986**, *108*, 2938–2939.
(55) Wu, R.; Arap Koske, S. K.; White, R. P.; Anson, C. E.; Jayasooriya, U. A.; Cannon, R. D. *J. Chem. Soc., Chem. Commun.* **1994**, 1657–1658.
(56) Sowrey, F. E.; MacDonald, C. J.; Cannon, R. D. *J. Chem. Soc., Faraday Trans.* **1998**, *94*, 1571–1574.
(57) Wu, R.; Poyraz, M.; Sowrey, F. E.; Anson, C. E.; Wocadlo, S.; Powell, A. K.; Jayasooriya, U. A.; Cannon, R. D.; Nakamoto, T.; Katada, M.; Sano, H. *Inorg. Chem.* **1998**, *37*, 1913–1921.
(58) Cannon, R. D.; Montri, L.; Brown, D. B.; Marshall, K. M.; Elliott, C. M. *J. Am. Chem. Soc.* **1984**, *106*, 2591–2594.
(59) *CrysAlis PRO*; Oxford Diffraction Ltd.: Abingdon, Oxfordshire, UK, 2007.
(60) Duisenberg, A. J. M.; Kroon-Batenburg, L. M. J.; Schreurs, A. M. M. *J. Appl. Crystallogr.* **2003**, *36*, 220–229.
(61) Blessing, R. H. *Acta Crystallogr. A* **1995**, *51*, 33–38.
(62) Sheldrick, G. M. *SHELXTL*; Bruker AXS: Madison, WI, USA, 2003.

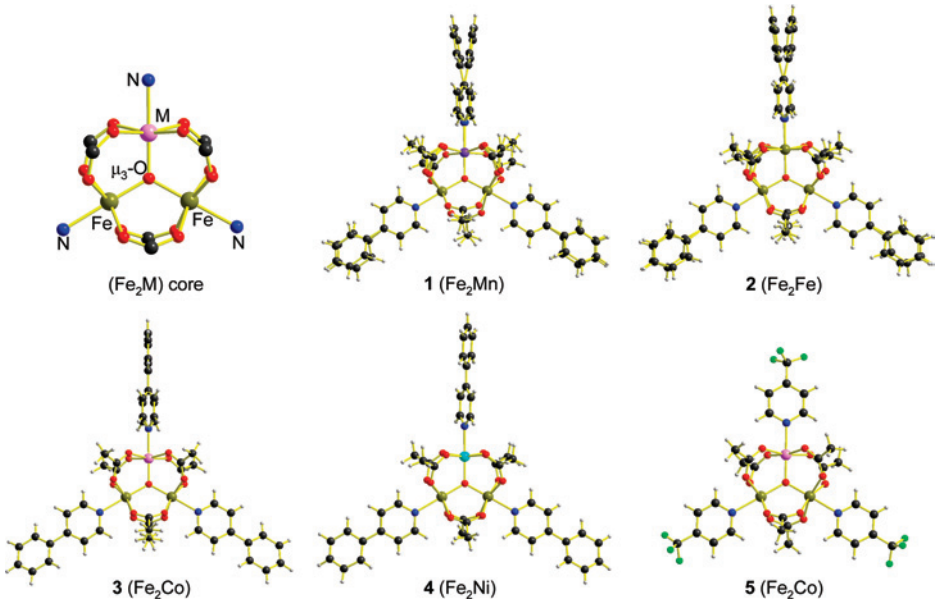

Figure 1. Crystal structures of $[Fe_2M(\mu_3\text{-}O)(\mu\text{-}O_2CCH_3)_6(4\text{-}Rpy)_3]$ complexes with M = Mn, Fe, Co, Ni and R = Ph, or CF_3.

coordinated ligands. The ^1H and ^{19}F NMR spectra were recorded on a Bruker DRX-400 spectrometer (9.4 T, resonance frequencies: 400.2 and 376.5 MHz, respectively). Typical spectral conditions for ^1H and ^{19}F NMR were 8k data points for the time domain, the spectrum window was set to 78 ppm, and the number of scans chosen was 32 and 512. The temperature was controlled within ±0.1 K using a Bruker BVT 3000 unit and was measured before or after spectral acquisition using a substitution method.[63] High-pressure high resolution spectra were monitored using a home-built narrow bore probe (5 mm NMR tube).[64]

2.4. NMR Data Analysis. Line widths and integrals of NMR signals were obtained by fitting Lorentzian functions to the experimental spectra using the "NMRICMA 3.0"[65] program for MATLAB. The adjustable parameters are the resonance frequency, intensity, line width, baseline, and phasing. Data analysis was carried out with the nonlinear least-squares fitting program VISUALIZEUR-OPTIMISEUR[66] for MATLAB, using the Levenberg-Marquard algorithm.

3. Results

3.1. X-ray Measurements. The oxo-centered trinuclear molecular structures of the series of new compounds $[Fe_2M(\mu_3\text{-}O)(\mu\text{-}O_2CCH_3)_6L_3]\cdot x(4\text{-Phpy})\cdot y(CH_3CN)$ **1**−**5** are reported in Figure 1. Crystallographic data, selected bond distances, and angles are presented in Tables 1 and 2. Beside the neutral trinuclear complex all crystals **1**−**5** contain variable amounts of acetonitrile and three of them **1**−**3** also contain noncoordinated 4-phenylpyridine.

The trinuclear skeletons are very similar to those of other trinuclear chromium(III) and iron(III) carboxylates.[34−36,55,57] The three metal ions lie at the corners of an isosceles, nearly equilateral, triangle with the Fe−M distances exceeding the Fe−Fe distance by 0.003 to 0.074 Å and with larger Fe−M−Fe than Fe−Fe−M angles by 0.1° to 2.2°. The centers of the Fe_2M triangles are occupied by a triply bridging oxygen which is not significantly displaced out of the plane (typically 0.02 Å). The trigonal symmetry at this μ_3-oxygen is reflected by the Fe−O−Fe and Fe−O−M angles close to 120°: the former exceeding the latter from 0.0° up to 5.0°. Interestingly, the largest observed deviations are for **2**(Fe_2Fe).

The μ_3-oxygen atom is the common vertex of the coordination octahedrons around the two Fe and the M heteroatoms. The acetates act as bidentate ligands and bridge couples of metal ions, so that four acetate oxygen atoms surround each metal ion. An examination of the angle values in the structures shows that all the $(\mu_3\text{-}O)\text{−}Fe\text{−}O_{Ac}$ and $(\mu_3\text{-}O)\text{−}M\text{−}O_{Ac}$ angles exceed 94°. This is also reflected by the $Fe\text{−}O_4$ plane (0.22−0.26 Å) and $M\text{−}O_4$ plane (0.13−0.21 Å) distances. A pyridine derivative molecule (4-Phpy or 4-CF_3py), in *trans* position to the shared oxo ligand, acts as the sixth donor. Coordination at each Fe^{III} and M^{II} ions

Table 2. Selected Structural Data (Bond Lengths [Å], Angles [°], Plane Deviations [Å] and Calculated Valence Bond Parameters V) for $[Fe_2M(\mu_3\text{-}O)(\mu\text{-}O_2CCH_3)_6(4\text{-}Rpy)_3]$, with M^{II} = Mn, Fe, Co, Ni, and R = Ph, CF_3

	1 (Fe_2Mn)[a]	**2** (Fe_2Fe)[a]	**3** (Fe_2Co)[b]	**4** (Fe_2Ni)[a]	**5** (Fe_2Co)[a]
Fe−N[c]	2.238(6)	2.228(3)	2.217(5)	2.200	2.219
M−N	2.263(4)	2.212(2)	2.227(6)	2.184(5)	2.211(5)
Fe−(μ_3-O)[c]	1.888(3)	1.844(1)	1.911(3)	1.882	1.894
M−(μ_3-O)	1.964(6)	2.021(2)	1.929(5)	1.926(4)	1.904(4)
O−Fe−O[c]	167.1	164.3	167.8	167.1	167.2
O−M−O[c]	170.4	170.2	168.7(2)	169.4	168.3
Fe−O−Fe[c]	121.4(3)	123.3(1)	120.5(3)	120.0(2)	119.8(2)
Fe−O−M[c]	119.3(2)	118.3(1)	119.8(1)	120.0	120.2(2)
$Fe\text{−}O_{Ac}$[c]	2.059	2.036	2.064	2.034	2.036
$M\text{−}O_{Ac}$[c]	2.085	2.116	2.068	2.050	2.051
$Fe\text{−}O_4$ plane	0.23	0.26	0.22	0.23	0.23
$M\text{−}O_4$ plane	0.17	0.13	0.20	0.19	0.21
(μ_3-O)−Fe_2M plane	0.02	0.02	0.02	0.01	0.04
V_M[d]	2.66	2.40	1.98	1.95	2.45
$V_{Fe(III)}$[d]	2.91	3.03	2.79	3.05; 3.07	2.96; 2.87

[a] Measured at 140(2) K. [b] Measured at 100(2) K. [c] Average values, unless s.d. reported. [d] Calculated according to refs 67 and 68.

(63) Ammann, C.; Meier, P.; Merbach, A. E. *J. Magn. Reson.* **1982**, *46*, 319–321.
(64) Cusanelli, A.; Nicula-Dadci, L.; Frey, U.; Merbach, A. E. *Inorg. Chem.* **1997**, *36*, 2211–2217.
(65) Helm, L.; Borel, A. *NMRICMA 3.0*; ISIC, EPFL: Lausanne, Switzerland, 2003.
(66) Yerly, F. *VISUALISEUR 3.5*; ISIC, EPFL: Lausanne, Switzerland, 2001.

Table 3. Structural Data (Bond Lengths [Å], Angles [°]) for Selected $[Fe^{III}_2Fe^{II}(\mu_3\text{-}O)(\mu\text{-}O_2CCH_3)_6(4\text{-}Rpy_3)]\Delta S$ Trinuclear Clusters

4-Rpy =	4-Phpy[a]	3-Clpy[b]	3-Clpy[b]	4-Etpy[c]	3-Etpy[d]	3-Etpy[d]
S =	0.35(4-Phpy)·3.3(CH_3CN)	3-Clpy	3-Clpy	4-Etpy	0.5 toluene	CH_3CCl_3
T(K)	140	122	122	163	298	238
Fe^{III}−N	2.228	2.255	2.245	2.23	2.251	2.235
Fe^{II}−N	2.212	2.228	2.223	2.224	2.251	2.227
Fe^{III}−(μ_3O)	1.844	1.852	1.846	1.856	1.862	1.884
Fe^{II}−(μ_3O)	2.021	2.107	2.02	2.01	2.006	1.937
Fe^{III}−O_{Ac}	2.036	2.038	2.041	2.048	2.045	2.052
Fe^{II}−O_{Ac}	2.116	2.11	2.1	2.11	2.107	2.078
O−Fe^{III}−O	164.3	165.3	165.4		166	167.8
O−Fe^{II}−O	170.2	173.7	173		173.2	170.4
Fe^{III}−O−Fe^{III}	123.3	124	123.3	123.3	122.7	121.1
Fe^{III}−O−Fe^{II}	118.3	118	118.4	118.4	118.6	119.5

[a] This work. [b] Two different crystals, ref 31. [c] Ref 30. [d] Ref 32.

includes five metal oxygen bonds and one metal−nitrogen bond in a slightly distorted octahedral (excentered metal-ion) environment.

In all X-ray structures reported for trinuclear clusters with two iron centers, the pyridine ligands are nearly parallel to or perpendicular to the Fe_2MO plane. All four possible isomers having 3, 2, 1 or 0 pyridine coplanar with the Fe_2MO plane have been reported.[29] In compound **1**−**4** the two 4-Phpy linked to the Fe are coplanar and the third one linked to M is perpendicular to the Fe_2MO plane. In compound **5** the three 4-CF_3py molecules are coplanar with the Fe_2CoO plane.

The localization of the divalent metal in the $M^{III}_2M^{II}O$ structures is not trivial and has been the subject of numerous discussions.[33] The above assignments mainly based on existing planes of symmetry along the N−M−(μ_3-O) axis is coherent with the bond distances and angles expected for Fe^{III} and M^{II} transition metal ions. We have also calculated the valence bond parameters (Table 2), which confirm these assignments.[67,68]

The understanding of the solid-state behavior of **2**(Fe_2Fe) is of particular interest for the interpretation of its NMR spectra in solution. Table 3 shows a comparison of this compound with other related $[Fe^{III}_2Fe^{II}(\mu_3\text{-}O)(\mu\text{-}O_2CCH_3)_6(Rpy_3)]\cdot S$ trinuclear clusters. It has been found that the two asymmetric isomers with 2 or 1 pyridine ligands in the Fe_3O plane exhibit ^{57}Fe−Mössbauer spectra (two doublets) characteristic of relatively valance-trapped species. As the temperature is increased, there is clearer evidence in the ^{57}Fe−Mössbauer spectra of an increasing rate of interconversion between the different vibronic states. The temperature dependence of spin-trapping is well established. An excellent parameter to describe the degree of spin-trapping is the difference between the Fe^{II}−(μ_3-O) and Fe^{III}−(μ_3-O) bond distances. From left to right in Table 3 these differences are 0.177, 0.255, 0.174, 0.154, 0.144, and 0.053 Å. This shows that our new compound **2**(Fe_2Fe) is well spin-trapped at 140 K and is an interesting candidate to possibly observe a Fe^{II}/Fe^{III} intramolecular electron transfer rate at low temperature in solution.

3.2. NMR Structure Analysis in Solution. The trinuclear heterometallic carboxylates $[Fe^{III}_2M^{II}(\mu_3\text{-}O)(\mu\text{-}O_2CCH_3)_6\text{-}(4\text{-}Rpy)_3]$ where R = Ph or CF_3 and M^{II} = Mn, Co or Ni, have a C_2 axis of symmetry involving chemically and magnetically nonequivalent coordinated pyridine type ligands and also nonequivalent bridging acetate ligands. Consequently, their NMR spectra should have separate signals for the Fe^{III} and M^{II} coordinated 4-Rpy protons and fluorines. The population ratio between these signals should be 2:1. Similarly, the Fe−Fe and Fe-M bridging acetate ligands should present two signals with a 1:2 population ratio.

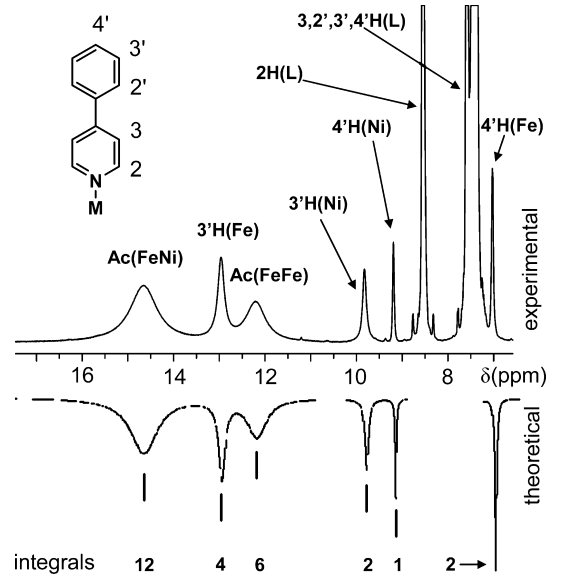

Figure 2. Fragment of experimental and theoretical ^{1}H NMR spectra (CD_2Cl_2, T = 192 K) of compound **4**(Fe_2Ni) (19.2 mM) with an excess of 4-Phpy (78.3 mM). The fitted spectrum is the sum of Lorentzian lines with the populations indicated in the figure.

A fragment of a typical ^{1}H NMR spectrum for $[Fe_2Ni(\mu_3\text{-}O)(\mu\text{-}O_2CCH_3)_6(4\text{-}Phpy)_3]$ (**4**), including the analysis of the population ratios is shown in Figure 2. The 192 K spectrum of **4** displays 10 paramagnetically shifted resonances (relative integrals in bracket) at 40.36 (2), 25.24 (4), 14.65 (12), 12.96 (4), 12.21 (6), 9.82 (2), 9.19 (1) and 7.02 (2) ppm. The signals at 14.65 and 12.21 ppm were assigned to the two different bridging acetate ligands Ac(FeNi) and Ac(FeFe). The signals at 25.24, 12.96, 7.02 ppm were assigned to 2′H(Fe), 3′H(Fe), 4′H(Fe) of 4-Phpy coordinated to the two Fe^{III} atoms and those smaller by a factor 2 at 40.36, 9.82 and 9.19 ppm were assigned to 2′H(Ni), 3′H(Ni) and 4′H(Ni) of 4-Phpy coordinated to the single Ni^{II} atom. The signals 2H and 3H of the coordinated 4-Phpy are too close to the paramagnetic centers to be observed. The doublet at 8.54 and the multiplets in the range 7.66−7.26 ppm belong to

(67) Liu, W.; Thorp, H. H. *Inorg. Chem.* **1993**, *32*, 4102–4105.
(68) Brese, N. E.; O'Keeffe, M. *Acta Crystallogr.* **1991**, *B47*, 192–197.

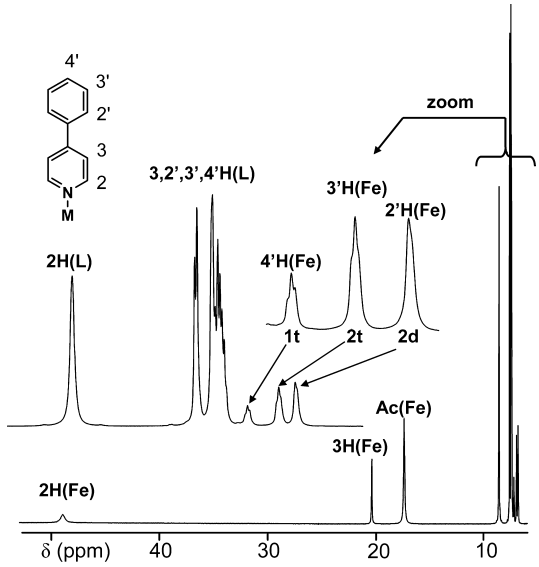

Figure 3. ^{1}H NMR spectrum of **2**(Fe_2Fe) (5.5 mM) with an excess of 4-Phpy (50.5 mM) at 234 K in CD_2Cl_2.

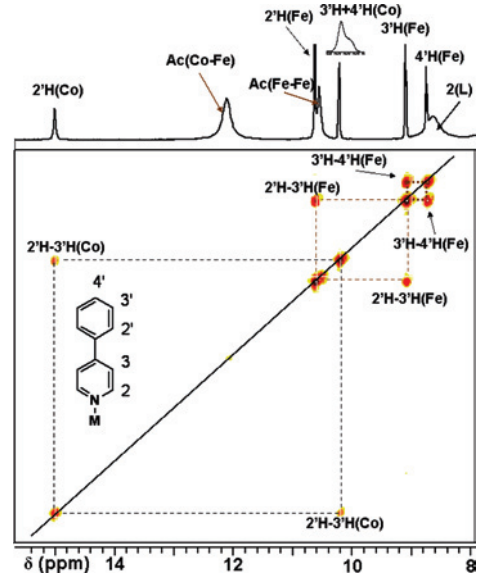

Figure 5. Fragment of COSY ^{1}H NMR spectrum of **3**(Fe_2Co) (20.3 mM) with an excess of 4-Phpy (110.1 mM) at 220 K in CD_2Cl_2.

the noncoordinated 4-Phpy added in excess in solution. In summary, in **4** a progressive decrease of the proton chemical shifts and transverse relaxation rates with the distance and the number of chemical bonds from the paramagnetic centers is observed. The temperature dependence of the spectra for **4**, with a typical paramagnetic behavior of the chemical shifts and of the transverse relaxation rates, is shown in Supporting Information, Figure S2.

In the mixed valence complex **2**(Fe_2Fe) it was not possible to observe separate signals for 4-Phpy coordinated to Fe^{III} and Fe^{II}, due to the fast intramolecular electron transfer process at the NMR time scale. Even at low temperature in CD_2Cl_2 only population averaged signals could be observed. A typical low temperature spectrum (234 K) is shown in Figure 3. In this case the signals assignment was achieved by taking advantage of (i) the characteristic splitting due nuclear spin−spin interaction at low temperature for outlying protons in the distant phenyl rings, (ii) the importance of the paramagnetic shifts and (iii) the values of the population ratios between acetate and 4-Phpy protons. The spectrum consists of seven signals (populations in parenthesis) with the following chemical shifts 48.45 (2), 20.47 (2), 17.42 (6), 8.58 (7), 7.17 (1), 6.92 (2), 6.76 (2) ppm and one group of multiplets in the range 7.63−7.35 (17.5). The phenyl protons 4′H(Fe), 3′H(Fe) and 2′H(Fe) corresponds to the signals at 7.17 (1H, t), 6.92 (2H, t) and 6.76 (2H, d), respectively. The spectrum of the acetate deuterated compound **2*** is similar to that of **2**, except the absence of the acetate signal Ac(Fe) at 17.42 ppm (Figure S3, Supporting Information). The signals at 48.45 and 20.47 ppm are assigned to the 2H(Fe) and 3H(Fe) pyridine protons, respectively. The signal at 8.58 and the group of multiplets at 7.63−7.35 ppm are assigned to the 2H and 3H, 2′H, 3′H, 4′H protons of the noncoordinated 4-Phpy ligand.

Some of the signals of **3**(Fe_2Co) show high and others low frequency paramagnetic shift changes with temperature (Figure 4). For the ^{1}H NMR spectral assignment of this compound we resort to ^{1}H−^{1}H COSY spectroscopy at 220 K (Figure 5). The signal localized at 9.09 ppm has cross peaks with two other signals at 10.60 and 8.67 ppm, which corresponds to the three protons of a phenyl ring. The two signals at 10.19 and 15.01 ppm display also cross-peaks. The integrals of the first group of signals (10.60, 9.09 and 8.67) are twice as large as the integrals of the second group of

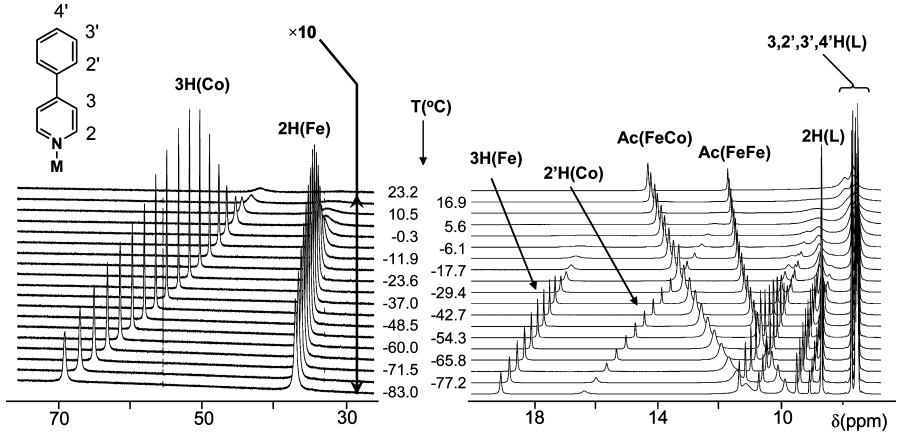

Figure 4. Temperature dependence of ^{1}H NMR spectra of **3**(Fe_2Co) (20.3 mM) with an excess of 4-Phpy (110.1 mM) in CD_2Cl_2 (8−16 ppm: see also Figure 5; 30−70 ppm is zoomed by a factor 10).

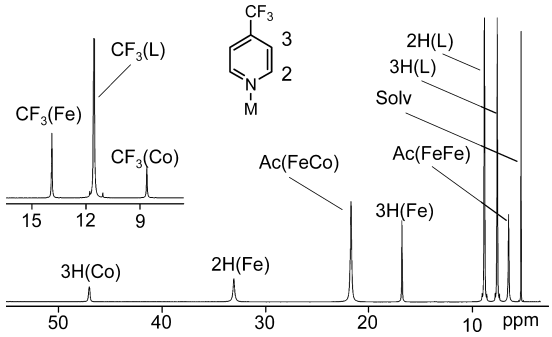

Figure 6. ^{1}H and ^{19}F (inset) NMR spectrum of **5**(Fe_2Co) (20.5 mM) with an excess of 4-CF_3py (68.0 mM) at 240 K in CD_2Cl_2.

signals (10.19; 15.01). Therefore, the first group can be assigned to the phenyl protons of 4-Phpy coordinated to Fe^{III} (2′H, 3′H, and 4′H) and the second group to those coordinated to Co^{II}. Through different evolution of the contact and the pseudocontact contributions to the chemical shift the signal of the 4′H(Co) proton is very close to that of the 3′H(Co) proton (see zoom in the Figure 5). The evolution of the line-width with increasing temperature of the Fe^{III} and Co^{II} coordinated 4-Phpy ligand shows the classical Curie behavior with line-narrowing (low temperature) and a line-broadening due to chemical exchange with free ligand (higher temperature). The signals for the Ac(FeCo) (12.13 ppm) and Ac(FeFe) (10.56 ppm) protons have an anti-Curie shift behavior[69] and as expected show no exchange broadening, which confirms the kinetic inertness of the central trinuclear core at the NMR time scale.

The ^{1}H NMR spectrum of **5**(Fe_2Co) at 240 K consists of five signals with the following chemical shifts: 47.04/3H(Co), 33.04/2H(Fe), 21.73/Ac(FeCo), 16.81/3H(Fe), 6.48/Ac(FeFe) ppm (Figure 6). The two intense signals at 8.82/2H(L) and 7.59/3H(L) ppm correspond to the noncoordinated ligand added to the solution. The signal of 2H(Co) pyridine has a chemical shift larger than 80 ppm and was not detected in this experiment. The ^{19}F NMR spectra (see inset of Figure 6) recorded at the same temperature shows three signals for the CF_3 group: 13.90/CF_3(Fe), 8.91/CF_3(Co), and 11.55 for free 4-CF_3py.

The NMR spectra of compound **1**(Fe_2Mn) shows very broad overlapping signals due to the slow electronic relaxation of high spin Mn^{II} in the $S = 5/2$ ($^6A_{1g}$) configuration (see Supporting Information, Figure S4). For this reason, NMR kinetic studies were not performed on this compound.

The signal assignments of the trinuclear clusters (**2**−**5**) have also been confirmed by the temperature evolution of the NMR transverse relaxation rates and by the resulting kinetic parameters (see kinetic part). Further the solution NMR investigation demonstrates the persistence in solution of the solid state X-ray determined structure of the heterometallic (**3**−**5**) and mixed valence (**2**) trinuclear clusters.

3.3. NMR Kinetics. In dichloromethane the exchange reactions between the 4-Rpy ligand coordinated in [$Fe^{III}_2M^{II}$-(μ_3-O)(μ-Ac)$_6$(4-Rpy)$_3$] and an excess of the 4-Rpy ligand are slow on the NMR time scale. This allows one to determine separately the exchange rates for 4-Rpy coordinated to the trivalent (eq 1) and to the divalent (eq 2) metal ions for compounds **3**(Fe_2Co), **4**(Fe_2Ni), and **5**(Fe_2Co).

$$[Fe_2M(\mu_3\text{-}O)(\mu\text{-}O_2CCH_3)_6(4\text{-}Rpy^{Fe})_2 4\text{-}Rpy^{M}] + 2{*}4\text{-}Rpy \rightleftharpoons [Fe_2M(\mu_3\text{-}O)(\mu\text{-}O_2CCH_3)_6({*}4\text{-}Rpy^{Fe})_2 + 4\text{-}Rpy^{M}] + 2\ 4\text{-}Rpy \quad (1)$$

$$[Fe_2M(\mu_3\text{-}O)(\mu\text{-}O_2CCH_3)_6(4\text{-}Rpy^{Fe})_2 4\text{-}Rpy^{M}] + {*}4\text{-}Rpy \rightleftharpoons [Fe_2M(\mu_3\text{-}O)(\mu\text{-}O_2CCH_3)_6(4\text{-}Rpy^{Fe})_2{*}4\text{-}Rpy^{M}] + {*}4\text{-}Rpy \quad (2)$$

Within the slow exchange approximation the observed transverse relaxation rate of the coordinated protons $1/T_2$ (= $\pi \times$ line-width) is the sum the paramagnetic line-broadening $1/T_{2m}$, dominant at low temperature, and $1/\tau$, dominant at high temperature (eq 3). The rate of exchange k of a particular ligand molecule is the inverse of its mean residence time τ in the coordinated site. The temperature dependence of $1/T_{2m}$ which incorporates dipolar and contact contributions is assumed to follow an Arrhenius behavior (eq 4). The temperature dependence of the kinetic contribution is described by the Eyring equation (eq 5).

$$\frac{1}{T_2} = \frac{1}{T_{2m}} + \frac{1}{\tau} = \frac{1}{T_{2m}} + k \quad (3)$$

$$\frac{1}{T_{2m}} = \frac{1}{T^{298}_{2m}} \exp\left[\frac{E_a}{R}\left(\frac{1}{T} - \frac{1}{298.15}\right)\right] \quad (4)$$

$$k = \frac{k_B T}{h} \exp\left[\frac{\Delta S^{\ddagger}}{R} - \frac{\Delta H^{\ddagger}}{RT}\right] = k^{298}\frac{T}{298.15} \times \exp\left[-\frac{\Delta H^{\ddagger}}{R}\left(\frac{1}{T} - \frac{1}{298.15}\right)\right] \quad (5)$$

The results of the fit of the transverse relaxation rates are shown in Figures 7−9 and the resulting kinetic parameters are reported in Table 4 (the paramagnetic relaxation parameters are given in Table S16, Supporting Information).

For the exchange of 4-Phpy coordinated to Fe^{III} in **3**(Fe_2Co) a simultaneous analysis of the transverse relaxation rates for 2H, 3H, 2′H protons was performed (Figure 7a). For the 4-Phpy coordinated to Co^{II} the $1/T_2$ temperature dependence is as expected monoexponential at low temperature for the 3H pyridine protons, but this is clearly not the case for the 2′H phenyl protons. The increase of the slope at low temperature of $\ln(1/T_2)$ for the 2′H protons is not of a simple paramagnetic relaxation (Figure 7b). For these protons we used a double exponential to better describe the paramagnetic contribution. This procedure does not affect the kinetic parameters which are well defined by the simultaneous fit of the relaxation data for 2′H(Co) and 3H(Co) (see Figure 7b).

The exchange of 4-Phpy coordinated to Fe^{III} (Figure 7c) and to Ni^{II} (Figure 7d) in **4**(Fe_2Ni) were both followed on the 2′H phenyl protons (Figure S1, Supporting Information). The paramagnetic broadening of the 2′H(Fe) signal is large, but with a negligible temperature dependence. The paramagnetic transverse relaxation rates of the proton of 4-Phpy

(69) Banci, L.; Bertini, I.; Luchinat, C.; Pierattelli, R.; Shokhirev, N. V.; Walker, F. A. *J. Am. Chem. Soc.* **1998**, *120*, 8472–8479.

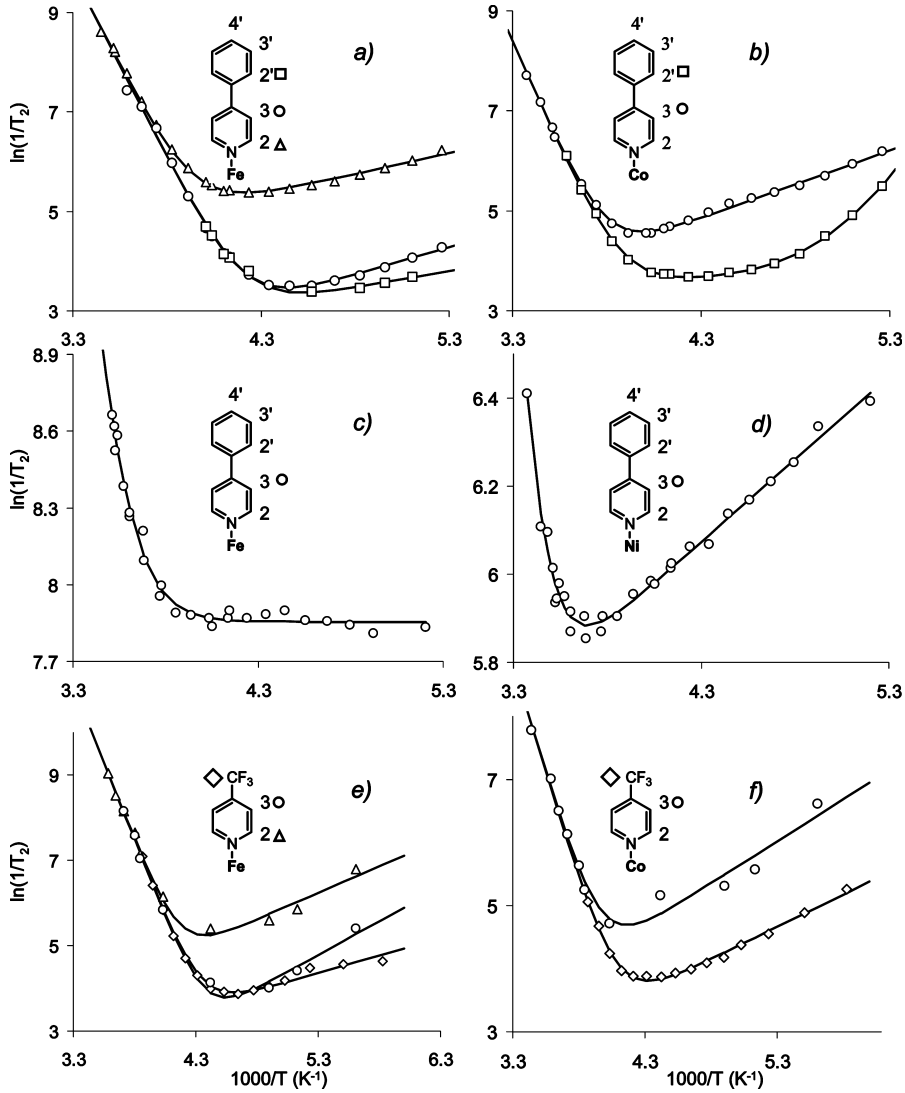

Figure 7. ^{1}H and ^{19}F transverse relaxation rates of coordinated ligand in CD_2Cl_2 solutions as a function of temperature: (a, b) **3**(Fe_2Co) (20.3 mM and 110.1 mM excess ligand), (c, d) **4**(Fe_2Ni) (19.2 mM and 78.3 mM), (e, f) **5**(Fe_2Co) (20.5 mM and 68.0 mM).

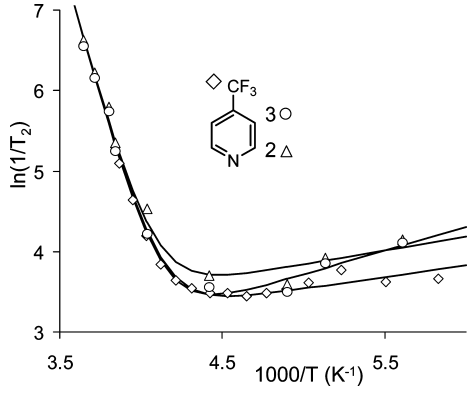

Figure 8. ^{1}H and ^{19}F transverse relaxation rates of free ligand in CD_2Cl_2 solutions of **5**(Fe_2Co) (20.5 and 68.0 mM) as a function of temperature.

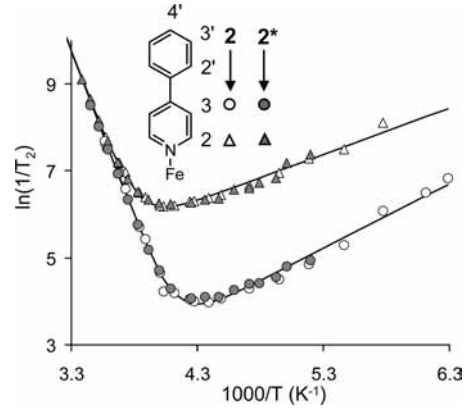

Figure 9. ^{1}H transverse relaxation rates of coordinated 4-Phpy in **2**(Fe_2Fe) (5.5 mM and 50.5 mM excess ligand) and **2***(Fe_2Fe) (18.6 and 120.1 mM) (Ac = CH_3COO^- and CD_3COO^-, in **2** and **2***, respectively) in CD_2Cl_2 as a function of temperature: solid lines are simultaneous least-squares fit to eqs 4, 5, and 9a.

coordinated to Fe^{III} in **3**(Fe_2Co) and **4**(Fe_2Ni) is strongly influenced by the nature of the divalent ion.

The cluster **5**(Fe_2Co) is particular in the sense that the 4-CF_3py ligand exchange was followed by ^{1}H and by ^{19}F NMR, on both the Fe^{III} and the Co^{II} centers (Figure 6). In this case we tested the coherence of the analysis not only by analyzing simultaneously the ^{1}H and ^{19}F coordinated ligand signals (Figure 7e,f), but also by adding the transverse relaxation rates $1/T_2^L$ of both nuclei (2H, 3H, and CF_3) for the free ligand (Figure 8). The exchange rate constants (rates of departure from the coordinated sites) k^{Fe} and k^{Co}, and the

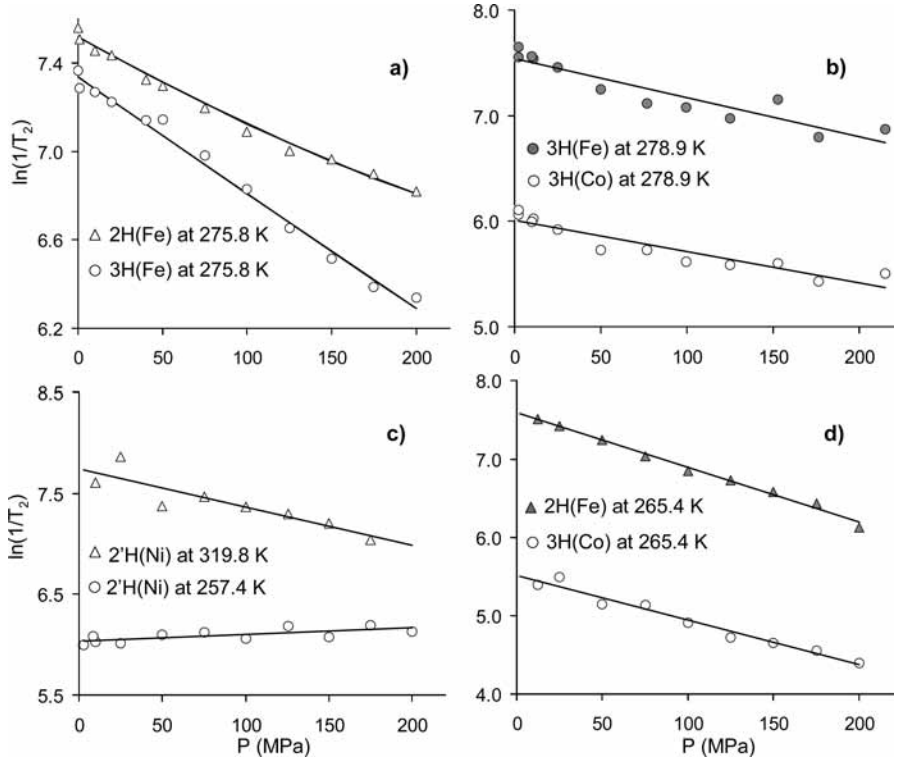

Figure 10. Pressure dependence of $\ln(1/T_2)$ for coordinated 4-Rpy from ^{1}H NMR for compounds (a) **2**(Fe_2Fe) (45.0 mM and 105.0 mM excess ligand); (b) **3**(Fe_2Co) (18.9 mM and 104.7 mM); (c) **4**(Fe_2Ni) (18.8 mM and 100.0 mM); (d) **5**(Fe_2Co) (265.4 mM and 68.0 mM) in CD_2Cl_2 solutions. Solid lines are simultaneous least-squares fit to eqs 10 and 11.

reverse rate constants (rates of departure from the free ligand site) $k^{L\text{-}Fe}$ and $k^{L\text{-}Co}$, are related by the populations of the ligand in these sites P_{Fe}, P_{Co}, and P_L through eq 6. The outer-sphere transverse relaxation term $1/T_{2os}$ (Arrhenius behavior) has been added to take into account the small distant interaction of the free ligand with the paramagnetic centers (eq 7). The excellent quality of the fits demonstrates the validity of the kinetic models and the absence of paramagnetic impurities in solution.

$$k^{L\text{-}Fe} = k^{Fe}\frac{P_{Fe}}{P_L} \text{ and } k^{L\text{-}Co} = k^{Co}\frac{P_{Co}}{P_L} \quad (6)$$

$$\frac{1}{T_2^L} = k^{L-Fe} + k^{L-Co} + \frac{1}{T_{2os}} \quad (7)$$

Because of the fast intramolecular electron transfer process at the NMR time scale it is not possible to separate the ligand exchange contribution on the Fe^{III} and Fe^{II} centers of **2**(Fe_2Fe). In this case the observed transverse relaxation rate of the average signals is related to the exchange rate constants ($k^{Fe(III)}$ and $k^{Fe(II)}$), the populations ($P_{Fe(III)} = 2/3$ and $P_{Fe(II)} = 1/3$) and the paramagnetic line-broadening ($1/T_{2m}^{Fe(III)}$ and $1/T_{2m}^{Fe(II)}$) of the two sites through eq 8.

$$\frac{1}{T_2} = P_{Fe(III)}\left(\frac{1}{T_{2m}^{Fe(III)}} + k^{Fe(III)}\right) + P_{Fe(II)}\left(\frac{1}{T_{2m}^{Fe(II)}} + k^{Fe(II)}\right) \quad (8)$$

Equation 8 has been simplified for three limiting cases: (1) $k^{Fe(III)} \gg k^{Fe(II)}$ (eq 9a), (2) $k^{Fe(III)} = k^{Fe(II)}$ (eq 9b), and (3) $k^{Fe(III)} \ll k^{Fe(II)}$ (eq 9c). It was assumed that the sum of the two paramagnetic contributions can be averaged in a single Arrhenius monoexponential contribution $1/T_{2m}^{Fe(III,II)}$. For **2**(Fe_2Fe), we compared the kinetic behavior of compounds **2** and **2***, synthesized with CH_3COO^- and CD_3COO^-, respectively.

$$\frac{1}{T_2} = \frac{1}{T_{2m}^{Fe(III,II)}} + \frac{2}{3}k^{Fe(III)} \quad (9a)$$

$$\frac{1}{T_2} = \frac{1}{T_{2m}^{Fe(III,II)}} + k^{Fe(III,II)} \quad (9b)$$

$$\frac{1}{T_2} = \frac{1}{T_{2m}^{Fe(III,II)}} + \frac{1}{3}k^{Fe(II)} \quad (9c)$$

As expected the paramagnetic relaxation behavior is the same for both compounds (low T) (Figure 9). What is more interesting is the identical kinetic behavior (high T), despite the 2.4 larger excess of free 4-Phpy for the experiment with the deuterated acetate. This is a proof for a first-order behavior for the ligand exchange reaction (first order in coordinated and zero-order in free ligand). The analysis for the three limiting cases gives, identical $1/T_{2m}^{298}$, E_a, and $\Delta H^{\ddagger}$ values, almost identical $\Delta S^{\ddagger}$ values, and the following rate constants at 298 K: $k^{Fe(III)} = 16.6 \pm 0.7 \times 10^3\ s^{-1}$, $k^{Fe(III,II)} = 11.1 \pm 0.5 \times 10^3\ s^{-1}$, $k^{Fe(II)} = 33.2 \pm 1 \times 10^3\ s^{-1}$. The differences in the k values stem from the different prefactors values in eqs 9a−9c and will be discussed below.

3.4. Variable Pressure NMR Kinetics. Measurements of the transverse relaxation rate of protons of the coordinated pyridines were performed as a function of pressure up to 200 MPa, at constant temperature, in order to determine the activation volumes $\Delta V^{\ddagger}$ for the pyridine exchange reactions (eqs 1 and 2) for compounds **2**−**5**. The pressure

has an effect on both components of $1/T_2$ (eq 3) as given by eqs 10 and 11.[5]

$$k = k^{P=0} \exp\left[-\frac{\Delta V^{\ddagger}}{RT}P\right] \quad (10)$$

$$\frac{1}{T_{2m}} = \frac{1}{T_{2m}^{P=0}} \exp\left[-\frac{\Delta V_m^{\ddagger}}{RT}P\right] \quad (11)$$

The variable pressure experiments were performed at high temperature to maximize the kinetic contribution k and minimize the paramagnetic contribution $1/T_{2m}$ (eq 3). The $\Delta V_m^{\ddagger}$ values are mainly related to the changes of viscosity and to the related changes of the rotational correlation time with pressure. In order to estimate separately the $\Delta V_m^{\ddagger}$ values, we analyzed the data of the acetate signals, free of kinetics contribution, for compounds **3**−**5** (Tables S14 and S15, Supporting Information). The resulting $\Delta V_m^{\ddagger}$ values range between -0.3 ± 1 and -3.0 ± 1 cm^3 mol^{-1} and their absolute values are much smaller than those of the $\Delta V^{\ddagger}$ values (see Table 4). In the $1/T_2(P)$ data fitting procedure we fixed $1/T_{2m}{}^{P=0}$ to the value calculated from the parameters obtained in the variable temperature study and left as single variables $k^{P=0}$ and $\Delta V_m^{\ddagger}$. In each case three fits were performed with $\Delta V_m^{\ddagger}$ values fixed at 0, −2 and −4 cm^3 mol^{-1}. The resulting $\Delta V^{\ddagger}$ values using 0 and −4 are within the range of the statistical error calculated with the $\Delta V_m^{\ddagger}$ value of −2 cm^3 mol^{-1} reported in Table 4. The least-squares fit of the $1/T_2$ values for compounds **2**−**5** at their Fe^{III} and M^{II} centers are shown in Figure 10. For **3**(Fe_2Co) and **5**(Fe_2Co) the paramagnetic contributions are very small and the clear linear decrease of $\ln(1/T_2)$ with pressure is a visual indication of positive activation volumes for the exchange processes. For **2**(Fe_2Fe) only one signal is observed for each ligand proton due to the fast Fe^{III}/Fe^{II} electron exchange. Here the effect of pressure was followed and analyzed simultaneously for the 2H and 3H protons of coordinated 4-Phpy. The difference in the observed $\ln(1/T_2)$ slopes is due to different paramagnetic contributions to the two signals. Note that the value of the activation volume is independent of the kinetic model chosen (eqs 9a−9c). For **4**(Fe_2Ni) the paramagnetic contributions to $1/T_2$ are very important (see Figure 7). The broad signal of the 3H proton of 4-Phpy coordinated to Fe^{III} was too small to be followed in the less sensitive high pressure probe. Measurements were performed on the Ni center at a low temperature (257.4 K) to have a direct access to $\Delta V_m^{\ddagger}$ and at the highest possible temperature (319.8 K) to have a maximum kinetic contribution. Both sets of data were analyzed simultaneously (Figure 10c).

4. Discussion

The interest in μ_3-oxo trinuclear clusters was driven in the past by the possibility to incorporate different metal ions and to create heterometallic and mixed valence species with original spectral and magnetic properties. The synthesis of this family of compounds is straightforward. The five prepared neutral clusters $[Fe^{III}{}_2M^{II}(\mu_3\text{-}O)(\mu\text{-}O_2CCH_3)_6(4\text{-}Rpy)_3]\cdot S$, with M^{II} = Mn, Fe, Co and Ni, contain three apical pyridine derivatives (R = Ph or CF_3) chosen to increase the solubility in the noncoordinating dichloromethane solvent used in the kinetic studies. Depending on the crystallization conditions acetonitrile solvent molecules and excess of 4-Rpy are also found disordered in the crystal lattice.

Until now, most of the investigated ligand exchange reactions on clusters were relatively slow processes, easy to follow by integration of increasing and/or decreasing NMR signals as a function of time, with rate constants less than 10^{-3} s^{-1} like: dinuclear Cr_2[70] Rh_2,[71,72] trinuclear Mo_3 and W_3,[19,73−79] trinuclear Ru_3 and Rh_3,[20,48−53,80] Cr_3,[46,47] Ta_6, Nb_6,[81,82] and decaniobate Nb_{10}.[83] Among labile clusters, water exchange was studied on trinuclear Mo_3,[77] on Al^{III} in MAl_{12} with M = Al, Ga and Ge,[15] and on Fe^{III} in $Mo_{72}Fe_{30}$ Keplerate.[84] In this paper we present the first examples of variable temperature and pressure NMR kinetic analyses of labile 3d heterometallic and mixed valence paramagnetic clusters $Fe^{III}{}_2M^{II}$ (M = Fe, Co, Ni). In contrast with already published fast kinetic studies those ligand exchanges are taking place at two different paramagnetic metal sites: one exchange at the Fe^{III} sites and the other at the divalent M ion site according to eqs 1 and 2. The rate constants and activation parameters for 4-Rpy exchange reactions on $[Fe^{III}{}_2M^{II}(\mu_3\text{-}O)(\mu\text{-}O_2CCH_3)_6(4\text{-}Rpy)_3]$, and solvent exchange on related trinuclear clusters and homoleptic octahedral complexes are reported in Table 4. The exchange rate constants on the heterometallic trinuclear clusters **3**−**5**, observed in dichloromethane, are in the slow line-broadening exchange domain on the NMR time scale which allowed determining separately the exchange rates on the trivalent Fe^{III} and on the divalent Co^{II} and Ni^{II} sites.

This separation is not possible for the mixed valence trinuclear cluster **2**(Fe_2Fe) due to the fast electron exchange between Fe^{III} and Fe^{II} at the NMR time scale. Even at the lowest temperatures one observes only a weighted average of the paramagnetic contributions from the Fe^{III} and Fe^{II} sites,

(70) Crimp, S. J.; Spiccia, L.; Krouse, H. R.; Swaddle, T. W. *Inorg. Chem.* **1994**, *33*, 465–470.
(71) Drljaca, A.; Spiccia, L.; Krouse, H. R.; Swaddle, T. W. *Inorg. Chem.* **1996**, *35*, 985–990.
(72) Drljaca, A.; Zahl, A.; Eldik, v. R. *Inorg. Chem.* **1998**, *37*, 3948–3953.
(73) Patel, A.; McMahon, M. R.; Richens, D. T. *Inorg. Chim. Acta* **1989**, *163*, 73–78.
(74) Patel, A.; Siddiqui, S.; Richens, D. T.; Harman, M. E.; Hursthouse, M. B. *J. Chem. Soc., Dalton Trans.* **1993**, 107–114.
(75) Kathirgamanathan, P.; Soares, A.; Richens, D. T.; Sykes, A. *Inorg. Chem.* **1985**, *24*, 2950–2954.
(76) Powell, G.; Richens, D. T. *Inorg. Chem.* **1993**, *32*, 4021–4029.
(77) Richens, D. T.; Pittet, P.-A.; Merbach, A. E.; Humanes, M.; Lamprecht, G. J.; Ooi, B.-L.; Sykes, G. *J. Chem. Soc., Dalton Trans.* **1993**, 2505–2511.
(78) Richens, D. T.; Helm, L.; Pittet, P.-A.; Merbach, A. E.; Nicolo, F.; Chapuis, G. *Inorg. Chem.* **1989**, *28*, 1394–1402.
(79) Houston, H. R.; Richens, D. T.; Casey, W. H. *Inorg. Chem.* **2006**, *45*, 7962–7967.
(80) Abe, M.; Sasaki, Y.; Nagasawa, A.; Ito, T. *Bull. Chem. Soc. Jpn.* **1992**, *65*, 1411–1414.
(81) Black, J. R.; Nyman, M.; Casey, W. H. *J. Am. Chem. Soc.* **2006**, *128*, 14712–14720.
(82) Balogh, E.; Anderson, T. M.; Rustad, J. R.; Nyman, M.; Casey, W. H. *Inorg. Chem.* **2007**, *46*, 7032–7039.
(83) Villa, E. M.; Ohlin, C. A.; Balogh, E.; Anderson, T. M.; Nyman, M. D.; Casey, W. H. *Angew. Chem., Int. Ed.* **2008**, *47*, 4844–4846.
(84) Balogh, E.; Todea, A. M.; Müller, A.; Casey, W. H. *Inorg. Chem.* **2007**, *46*, 7087–7092.

Table 4. Rate Constants and Activation Parameters for 4-Rpy (R = Ph, CF_3) Exchange in $[Fe_2M(\mu_3\text{-}O)(\mu\text{-}O_2CCH_3)_6(4\text{-Rpy})^{Fe}_2(4\text{-Rpy})^{M}]$ where R = Ph for **2**(Fe_2Fe), **3**(Fe_2Co), **4**(Fe_2Ni), and R = CF_3 for **5**(Fe_2Co), and Solvent Exchange in Related Trinuclear and Homoleptic Octahedral Complexes[a]

compounds	solv	k^{298} s^{-1}	$\Delta H^{\ddagger}$ kJ mol^{-1}	$\Delta S^{\ddagger}$ J K^{-1} mol^{-1}	$\Delta V^{\ddagger}$ cm^3 mol^{-1}	mechanism	ref
$[Fe(H_2O)_6]^{3+}$	H_2O	1.6×10^2	64.0	+12.1	−5.4	I_a	85, 86
$[Fe(DMSO)_6]^{3+}$	DMSO	9.3	62.5	−16.7	−3.1	I_a	87
$[Fe(DMF)_6]^{3+}$	DMF	6.3×10^1	42.3	−69.0	−0.9	I	87
2($Fe^{III}_2Fe^{II}$)	CD_2Cl_2	$16.6 \pm 0.7 \times 10^3$	60.32 ± 1	$+34.8 \pm 4$	$+12.5 \pm 0.3$	D	this work
3($Fe^{III}_2Co^{II}$)	CD_2Cl_2	$11.9 \pm 0.4 \times 10^3$	58.92 ± 0.6	$+30.7 \pm 2$	$+10.6 \pm 1.5$	D	this work
4($Fe^{III}_2Ni^{II}$)	CD_2Cl_2	$12.2 \pm 1 \times 10^3$	67.91 ± 5	$+61.0 \pm 17$	−	D	this work
5($Fe^{III}_2Co^{II}$)	CD_2Cl_2	$46 \pm 4 \times 10^3$	58.21 ± 2	$+39.6 \pm 3$	$+14.2 \pm 1$	D	this work
$[Cr(H_2O)_6]^{3+}$	H_2O	2.4×10^{-6}	108.6	+11.6	−9.6	I_a	88
$[Cr(DMF)_6]^{3+}$	DMF	3.3×10^{-7}	97.1	−43.5	−6.3	I_a	89
$[Cr(DMSO)_6]^{3+}$	DMSO	3.1×10^{-8}	96.7	−64.5	−11.3	I_a	90
$[Cr_3O(Ac)_6(H_2O)_3]^{+b}$	DMA	520	107	+51	+9.6	D	46
$[Cr_3O(Ac)_6(Py)_3]^{+}$	CH_3NO_2	1.32×10^{-5}	127	+88	+10.2	D	47
$[Rh(H_2O)_6]^{3+}$	H_2O	2.2×10^{-9}	131	+29	−4.2	I_a	91, 92
$[Rh_3O(Ac)_6(H_2O)_3]^{+}$	H_2O	5.0×10^3	99	+43	+5.3	I_d	51
$[Fe(H_2O)_6]^{2+}$	H_2O	4.4×10^6	41.4	+21.2	+3.8	I_d	85, 86
$[Fe(MeCN)_6]^{2+}$	MeCN	5×10^4	50.2	+12.6	+0.4	I	87
$[Fe(DMF)_6]^{2+}$	DMF	9.7×10^5	43.0	+13.8	+8.5	I_d	87
$[Co(H_2O)_6]^{2+}$	H_2O	3.2×10^6	46.9	+37.2	+6.1	I_d	87
$[Co(DMSO)_6]^{2+}$	DMSO	4.5×10^5	49	+28	−	I_d	93
$[Co(DMF)_6]^{2+}$	DMF	3.9×10^5	56.9	+52.7	+6.7	I_d	87, 94
$[Co(MeCN)_6]^{2+}$	MeCN	3.4×10^5	49.5	+27.1	+8.1	I_d	87, 95, 96
$[Co(pa)_6]^{2+}$	pa	2.0×10^8	36.2	+35	−	I_d	97
3(Fe^{III}_2**Co^{II}**)	CD_2Cl_2	$2.8 \pm 0.1 \times 10^3$	68.24 ± 2	$+49.8 \pm 5$	$+13.9 \pm 2$	D	this work
5(Fe^{III}_2**Co^{II}**)	CD_2Cl_2	$4.7 \pm 0.5 \times 10^3$	55.37 ± 2	$+11.2 \pm 8$	$+10.9 \pm 1.5$	D	this work
$[Ni(H_2O)_6]^{2+}$	H_2O	3.2×10^4	56.9	+32	+7.2	I_d	98
$[Ni(DMF)_6]^{2+}$	DMF	3.8×10^3	62.8	+33.5	+9.1	D	87, 94, 99
$[Ni(MeCN)_6]^{2+}$	MeCN	2.8×10^3	64.3	+37	+8.5	I_d	87, 100
4(Fe^{III}_2**Ni^{II}**)	CD_2Cl_2	$3.7 \pm 0.2 \times 10^2$	78.62 ± 6	$+67.8 \pm 22$	$+12.3 \pm 2$	D	this work

[a] DMA = dimethylacetamide; DMF = dimethylformamide; DMSO = dimethylsulfoxide; MeOH = methanol, pa = *n*-propylamine. [b] Substitution of H_2O by DMA.

and no extra line broadening due to a kinetic fast exchange $\Delta\omega^2/k$ term ($\Delta\omega$ is the difference in the resonance frequencies between both Fe sites). In other words, the signals are kinetically totally coalesced for the intramolecular electron transfer process even down to 159 K (see also Figure 3). Above 240 K the coalesced signals start to broaden due to the intermolecular exchange of coordinated 4-Rpy with free one. NMR spectroscopy does not permit the assignment of this process to the exchange from the Fe^{III} or/and Fe^{II} site(s), and recourse has to be made to other arguments. The X-ray data of **5**(Fe_2Fe) shows an important spin trapping in the solid-state structure at 140 K (Figure 11). The differences between the Fe^{III} and Fe^{II} distances in this compound are much larger than those observed between Fe^{III} and M^{II} in compounds **1**, **3**, and **5**. A direct indicator of spin trapping, beside the structural data shown in Table 3, is Mössbauer spectroscopy. The Mössbauer spectra for the analogue compound $[Fe_2Fe(\mu_3\text{-}O)(\mu\text{-}O_2CCH_3)_6(py)_3]$ from 120 to 315 K consist of two quadrupole-split doublets in a 2:1 ratio. The more intense doublet is for the two Fe^{III}, whereas the other doublet arises from the single Fe^{II}. Oh et al.[29,30] conclude to an intramolecular electron-transfer rate $\leq 10^7$ s^{-1}. In contrast the Mössbauer spectrum of the py solvate of $[Fe_2Fe(\mu_3\text{-}O)(\mu\text{-}O_2CCH_3)_6(py)_3](py)$ shows a pronounced temperature dependence. At temperatures below $\approx$ 100 K the two doublets characteristic of high spin Fe^{III} and Fe^{II} are observed. As the temperature increase the spectrum changes to become a simple averaged doublet above $\approx$ 200 K. A temperature coalescence of the spectrum of the benzene solvate is also observed. The lattice surrounding the complex dramatically affects the intramolecular electron-transfer rate in this homometallic mixed-valence cluster in the solid state.

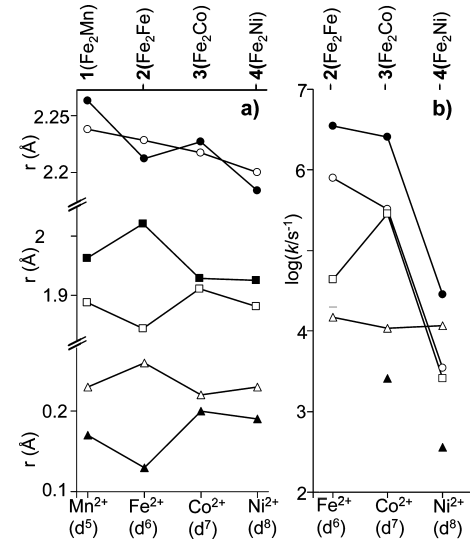

Figure 11. (a) Distances in compounds **1**−**4**: Fe^{III}−N (○) and M^{II}−N (●), Fe^{III}−(μ_3-O) (□) and M^{II}−(μ_3-O) (■), Fe^{III}−O_4 plane (Δ) and M^{II}−O_4 plane (▲) (140 K, except 100 K for **3**); (b) Rate constants for neat solvent exchange on $[MS_6]^{2+}$ (S=H_2O (●), DMF (○) and MeCN (□); and for 4-Phpy exchange at Fe^{III}(Δ) and M^{II}(▲) sites of compounds **2**−**4** in dichloromethane at 298 K.

This observation is consistent with the fast exchange rate observed for **2**(Fe_2Fe) in dichloromethane solution. The important deformation of the Fe_3 unit of **2**(Fe_2Fe) from an equilateral to an isosceles triangle in the solid state is due to the higher affinity of Fe^{III} for the hard oxygen and of Fe^{II} for the softer nitrogen. This property has been exploited by Shanzer et al.[101,102] to propose a molecular switch based on

(85) Grant, M. W.; Jordan, R. B. *Inorg. Chem.* **1981**, *20*, 55–60.

redox chemical triggering of iron translocation in triple helix complexes. In our case, the short $Fe^{III}-(\mu_3\text{-}O)$ distance (1.844(1) Å) induces a strong *trans*-bond weakening effect and therefore a long $Fe^{III}-N$ bond distance (2.228(3) Å). At the opposite the longer Fe^{II}-$(\mu_3$-O) distance (2.021(3) Å) produces a smaller *trans*-bond weakening effect and a relatively shorter $Fe^{II}-N$ bond distance (2.212(2) Å). Therefore for the following reasons, we favor a faster 4-Rpy exchange on the Fe^{III} site than on the Fe^{II} site of **2**(Fe_2Fe): (i) larger *trans* μ_3-O bond weakening, (ii) stronger steric and electronic repulsion of the pyridine N with respect of the four carboxylate oxygens as measured by the $Fe^{III}-O_4$ plane (0.26 Å) and $Fe^{II}-O_4$ plane (0.13 Å) distances and (iii) comparison of the variation of log *k* values for octahedral solvento-ions from Co^{II} to Fe^{II} (Figure 11).

It is now well accepted that the water exchange for high spin divalent and trivalent 3d octahedral aqua ions changes from the I_a to the I_d mechanism after the d^5 configuration. Because of the nonavailability of a rate-law in neat water the assignment was mainly based on the values and sign of the activation volumes along the series, and later confirmed by theoretical calculations. For the 4-Rpy exchanges on the Ni^{II} site of **4**(Fe_2Ni) and the Co^{II} site of **3**(Fe_2Co) and **5**(Fe_2Co) the $\Delta V^{\ddagger}$ values lie between +10.9 and +13.9 cm^3 mol^{-1}. These highly positive values are expected for $N_{Rpy}-M^{II}$ bond-breaking activation steps for late 3d high spin d^8 and d^7 metal centers. This has always been observed for hexacoordinated mononuclear Ni^{2+} and Co^{2+} ions in different solvent. A priori the assignment of the 4-Phpy exchange mechanism at the Fe^{3+} center is less obvious. The solvent exchange mechanism on $[Fe(H_2O)_6]^{3+}$ ($\Delta V^{\ddagger} = -5.4$ cm^3 mol^{-1}) is clearly I_a, but the associative character is decreasing for $[Fe(DMSO)_6]^{3+}$ (-3.1 cm^3 mol^{-1}) and further for $[Fe(DMF)_6]^{3+}$ (-0.9 cm^3 mol^{-1}), leading to the assignment of an I mechanism for the latter solvate. In the clusters studied the $\Delta V^{\ddagger}$ values for 4-Rpy exchange at the Fe^{III} site lie between +10.6 and +14.2 cm^3 mol^{-1}, and the activation entropies between +30.7 and + 61.0 J K^{-1} mol^{-1}, all values leading to the assignment of a dissociative d activation mode. The exchange rate at the Fe^{III} center of compound **2**(Fe_2Fe) was found independent of the concentration of the free ligand 4-Phpy. Further for compounds **3**(Fe_2Co) and **5**(Fe_2Co) traces of clusters (less than 15% in total) with partially dissociated 4-Rpy ligand could be observed in solution in the absence of added free ligand. Tentative assignments of these traces for **3**(Fe_2Co) show the presence of four clusters (b−e in Figure 12), in which 4-Phpy was partially substituted by solvent molecules, especially by acetonitrile which is contained as crystallization solvent in the synthesized compounds. The bottom spectrum of Figure 12 shows that the excess of pyridine type ligand shifts the equilibrium and suppresses the dissociation. In these excess ligand conditions the amounts of dissociated forms are very small (not detectable by NMR) and could therefore be neglected in the NMR kinetic analysis. All these observations together allow concluding to a limiting dissociative D mechanism at the three metal centers Co^{II}, Ni^{II}, and Fe^{III}.

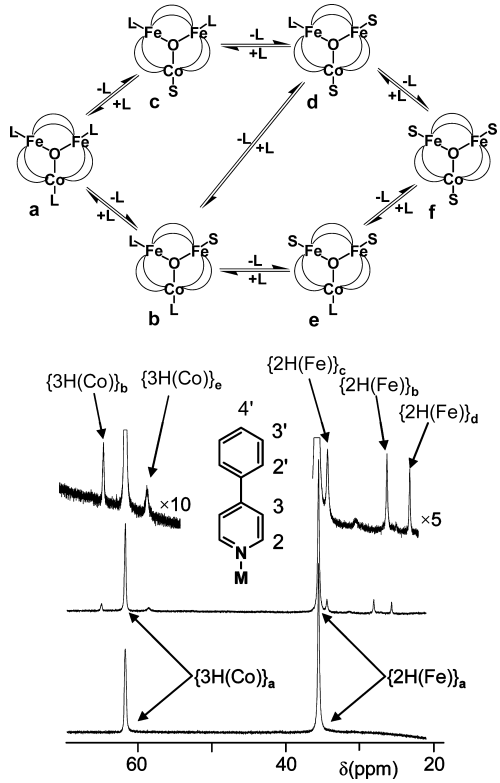

Figure 12. Dissociation pathways of **3**(Fe_2Co) and fragment of the ^1H NMR spectra of 20.3 mM **3**(Fe_2Co) at 220 K in CD_2Cl_2 with 110.1 mM excess (bottom) and without excess (top) of 4-Phpy ligand.

The exchange rates of the 4-Rpy ligand coordinated to Fe^{III} in the four clusters are 2−3 orders of magnitude faster in comparison with the mononuclear Fe^{3+} ion coordinated to six oxygen donor solvent molecules (H_2O, DMSO, and DMF). Similar increase of reactivity were found in mononuclear and in trinuclear species. For example the increase of water exchange from $[Al(H_2O)_6]^{3+}$ (1.29 s^{-1}), to $[Al(H_2O)_5F]^{2+}$ (0.23×10^3 s^{-1}) and $[Al(H_2O)_4F_2]^{+}$ (1.71×10^4 s^{-1}) is function of the decrease of charge of the

(86) Swaddle, T. W.; Merbach, A. E. *Inorg. Chem.* **1981**, *20*, 4212–4216.
(87) Meyer, F. K.; Newman, K.; Merbach, A. E. *J. Am. Chem. Soc.* **1979**, *101*, 5588–5592.
(88) Xu, F. C.; Krouse, H. R.; Swaddle, T. W. *Inorg. Chem.* **1985**, *24*, 267–270.
(89) Lo, S.; Swaddle, T. W. *Inorg. Chem.* **1975**, *14*, 1878–1881.
(90) Carle, D. L.; Swaddle, T. W. *Can. J. Chem.* **1973**, *51*, 3795–3798.
(91) Laurenczy, G.; Rapaport, I.; Zbinden, D.; Merbach, A. E. *Magn. Reson. Chem.* **1991**, S45–S51.
(92) De Vito, D.; Weber, J.; Merbach, A. E. *Inorg. Chem.* **2004**, *43*, 858–864.
(93) McAteer, C. H.; Moore, P. *J. Chem. Soc., Dalton Trans.* **1983**, 353–357.
(94) Matwiyoff, N. A. *Inorg. Chem.* **1966**, *5*, 788–795.
(95) Monnerat, A. R.; Moore, P.; Newman, K.; Merbach, A. E. *Inorg. Chim. Acta* **1981**, *47*, 139–145.
(96) Aizawa, S.; Matsuda, K.; Tajima, T.; Maeda, M.; Sugata, T.; Funahashi, S. *Inorg. Chem.* **1995**, *34*, 2042–2047.
(97) Aizawa, S.; Iida, S.; Matsuda, K.; Funahashi, S. *Inorg. Chem.* **1996**, *35*, 1338–1342.
(98) Ducommun, Y.; Newman, K. E.; Merbach, A. E. *Inorg. Chem.* **1980**, *19*, 3696–3703.
(99) Luz, Z.; Meiboom, S. *J. Chem. Phys.* **1964**, *40*, 2686–2693.
(100) Yano, Y.; Fairhurst, M.; Swaddle, T. W. *Inorg. Chem.* **1980**, *19*, 3267–3270.
(101) Zelikovich, L.; Libman, J.; Shanzer, A. *Nature* **1995**, *374*, 790–792.
(102) Constable, E. C. *Nature* **1995**, *374*, 760–761.

complexes, and of the *trans* effect produced by the F^- ion.[103] A similar effect was wound for $[M(H_2O)_6]^{3+}$ and $[M(H_2O)_5OH]^{2+}$ with M^{III} = Al,[104] Ga,[105] Fe,[85,86] Cr,[88] Ru,[106] Rh,[91] and Ir.[107] In the Fe^{III} case the replacement of a water molecule by an OH^- anion produces a 750 times increase of the water exchange rate and also a changeover from an I_a ($\Delta V^{\ddagger} = -5.4$ cm^3mol^{-1}) to an I_d ($\Delta V^{\ddagger} = +7.0$ cm^3 mol^{-1}) interchange mechanism. The inert $[Cr(H_2O)_6]^{3+}$ ($\Delta V^{\ddagger} = -9.6$ cm^3 mol^{-1}) and $[Rh(H_2O)_6]^{3+}$ ($\Delta V^{\ddagger} = -4.2$ cm^3mol^{-1}) aqua ions exchange water according to I_a mechanisms, but incorporated in trinuclear clusters this trivalent ions react according to dissociative mechanisms: $[Cr_3(\mu_3\text{-}O)(\mu\text{-}O_2CCH_3)_6(H_2O)_3]^+$ (D, $\Delta V^{\ddagger} = +9.6$ cm^3 mol^{-1}), $[Cr_3(\mu_3\text{-}O)(\mu\text{-}O_2CCH_3)_6(py)_3]^+$ (D, $\Delta V^{\ddagger} = +10.2$ cm^3 mol^{-1}) and $[Rh_3(\mu_3\text{-}O)(\mu\text{-}O_2CCH_3)_6(H_2O)_3]^+$ (I_d, $\Delta V^{\ddagger} = +5.3$ cm^3 mol^{-1}). Similarly the dissociative D mechanism for the exchange reaction at the Fe^{III} centers of compounds **2**−**5** is due to the strong *trans* effect induced by the short Fe^{III}−(μ_3-O) and the corresponding weakening of the Fe^{III}−N bond favoring dissociation. This bond weakening is also reflected by the Fe−O_4 plane deviation (0.22−0.24 Å) and the O_{ac}−Fe−N angles (82.0° for **2**(Fe_2Fe) and 83.6−83.9° for **3**−**5**). The rate constants are the same for **3**(Fe_2Co) and **4**(Fe_2Ni) with a small 1.4 times increase for spin-trapped compound **2**(Fe_2Fe). The 4 times increase in reactivity of **5**(Fe_2Co) compared to **3**(Fe_2Co), is due to the lower basicity of 4-CF_3py compared to 4-Phpy (gas-phase basicity (kJ mol^{-1}) and calculated charge at the N, with the following sequence: 4-Phpy (907.8/−0.261) > Py (898.1/−0.260) > 4-CF_3py (862.0/−0.239).[108,109]

The heterometallic trinuclear compounds give an opportunity to compare the reactivity of Fe^{III} and M^{II} ions (Fe, Co and Ni) in the same environment. Whereas the reactivity of Fe^{III} increases by 2−3 orders of magnitude, the reactivity decreases strongly for the M^{II} ions compared to the mononuclear solvates: $10-10^2$ for Ni^{II}, 10^2-10^5 for Co^{II} and ≥2 for Fe^{II}. For substitution reactions on divalent 3d transition metal ions the order of reactivity is $Cu^{2+} > Mn^{2+} > Fe^{2+} > Co^{2+} > Ni^{2+} > V^{2+}$. This order is also reflected in the values of the stability constants for the formation in water of the $[M(Py)(H_2O)_5]^{2+}$ complexes: Mn^{2+} (0.14) < Fe^{2+} (0.6) < Co^{2+} (1.14) < Ni^{2+} (1.78).[110] More stable is the complex, smaller will be the rate of breaking of the metal−nitrogen bond. This order, even if the rate constants are smaller is preserved for the 4-Phpy exchange rates: $Co^{2+} > Ni^{2+}$. For **3**(Fe_2Co) and **5**(Fe_2Co), similarly to the observation made for the Fe^{III} center, one observes an increase in reactivity when replacing 4-Phpy by the less basic 4-CF_3py ligand.

5. Conclusions

Five μ_3-oxo trinuclear clusters **1**−**5** were synthesized and structurally characterized by single crystal X-ray diffraction. The persistence of the structure of compound **2**−**5** in dichloromethane solution in the temperature range 190−320 K was demonstrated by ^1H and ^{19}F NMR spectroscopy. Even at the lowest temperature, the electron exchange in the homometallic mixed-valence compound **2**(Fe_2Fe) is in the fast regime at the NMR time scale. The full assignment of the NMR signals gave the opportunity to perform a unique selective kinetic analysis of the fast ligand exchanges at the two different labile metal centers in these clusters. A limiting D mechanism is assigned to these exchange reactions. This mechanism assignment is based on a first-order rate law, the detection of intermediates, the positive and large entropies and volumes of activation.

The observation of a D mechanism at the Ni^{II} and Co^{II} centers with a higher reactivity at the latter is consistent with the expectation for d^7 and d^8 ions. This reactivity is much lower than the reactivity of their oxygen donor solvates due the higher affinity of these ions for the 4-Rpy nitrogen donor atoms. On the contrary at the Fe^{III} center, the exchanges which are slow and usually associative if it surrounded by oxygen donors, become dissociative and faster than the two divalent ions in the cluster due to the weak bonding affinity of Fe^{III} for nitrogen donors. Interestingly, we do not observe a significant effect of the divalent metal ion in the cluster (Fe, Co and Ni) on the exchange rate of 4-Phpy at the Fe^{III} center, which seems to indicate that the electronic interactions between the three ions making the clusters do not influence the Fe^{III}−N bond strength. On the other hand, the paramagnetic chemical shifts and relaxation rates of the 4-Phpy protons coordinated to the Fe^{III} center are strongly affected by the nature of the divalent ion.

Acknowledgment. This work was supported by the Swiss National Science Foundation and the SCOPES (Scientific Cooperation between Eastern Europe and Switzerland) program. G.N. thanks the A. von Humboldt Foundation for support.

Supporting Information Available: ORTEP representation of the X-ray structures. NMR spectra. Tables of the $1/T_2$ variable temperature and variable pressure NMR data and results of the fitting of these data. This material is available free of charge via the Internet at http://pubs.acs.org.

IC801206M

(103) Yu, P.; Phillips, B. L.; Casey, W. H. *Inorg. Chem.* **2001**, *40*, 4750–4754.
(104) Nordin, J. P.; Sullivan, D. J.; Phillips, B. L.; Casey, W. H. *Inorg. Chem.* **1998**, *37*, 4760–4763.
(105) Hugi-Cleary, D.; Helm, L.; Merbach, A. E. *J. Am. Chem. Soc.* **1987**, *109*, 4444–4450.
(106) Rapaport, I.; Helm, L.; Merbach, A. E.; Bernhard, P.; Ludi, A. *Inorg. Chem.* **1988**, *27*, 873–879.
(107) Hugi, A. D.; Helm, L.; Merbach, A. E. *Helv. Chim. Acta* **1985**, *68*, 508–521.
(108) Hunter, E. P. L.; Lias, S. G. *J. Phys. Chem. Ref. Data* **1998**, *27*, 413–428.
(109) Sizova, O. V.; Ivanova, N. V.; Sizov, V. V.; Ershov, A. Y.; Baranovski, V. I. *Inorg. Chim. Acta* **2004**, *357*, 354–360.
(110) Bjerrum, J. *Acta Chem. Scand.* **1973**, *27*, 970–976.